

See discussions, stats, and author profiles for this publication at: <https://www.researchgate.net/publication/232250907>

Numerical Simulation of Multifuel Combustion in a 200 MW Tangentially Fired Utility Boiler

ARTICLE *in* ENERGY & FUELS · JANUARY 2012

Impact Factor: 2.79 · DOI: 10.1021/ef201149p

CITATIONS

17

READS

97

5 AUTHORS, INCLUDING:



Huaichun Zhou

Tsinghua University

148 PUBLICATIONS 1,195 CITATIONS

SEE PROFILE

Numerical Simulation of Multifuel Combustion in a 200 MW Tangentially Fired Utility Boiler

Qingyan Fang,[†] Amir A. B. Musa,[†] Yan Wei,[‡] Zixue Luo,[†] and Huaichun Zhou^{*,†}

[†]State Key Laboratory of Coal Combustion, Huazhong University of Science and Technology, Wuhan 430074, People's Republic of China

[‡]Department of Mechanical, Materials, and Aerospace Engineering, University of Central Florida, Orlando, Florida 32816-2450, United States

ABSTRACT: A computational fluid dynamics (CFD) model of a 200 MW multifuel tangentially fired boiler has been developed using Fluent 6.3.26, which is able to model the three-fuel combustion system of coal, blast furnace gas (BFG), and coke oven gas (COG) with an eddy-dissipation model for simulating the gas-phase combustion. A level of confidence in the current CFD model has been established by carrying out a mesh independence test and validation against the experimental data obtained from the boiler for case study. The validated CFD model is then applied to investigate the effects of different BFG and COG flow rates on the boiler performance. It is found that increasing the BFG flow rate brings negative effects on the ignition of primary air and pulverized-coal mixture, pulverized-coal burnout, and heat transfer in the furnace and, consequently, decreases the thermal efficiency. However, increasing the COG flow rate can increase the thermal efficiency via improving the pulverized-coal burnout and heat transfer. Increasing both the BFG and COG flow rates is favorable for reducing NO emissions. The results also indicate that co-firing pulverized coal with BFG of about 20% heat input and COG of about 10% heat input is an optimal operating condition for improving the boiler performance at 180 MW load. The present study provides helpful information for understanding and optimizing the multifuel combustion of the boiler.

1. INTRODUCTION

Blast furnace gas (BFG) and coke oven gas (COG), which are byproducts of the iron and steel manufacturing processes in the iron and steel industries, are important secondary energy sources.^{1–6} The BFG mainly contains N₂, CO₂, and CO and slight amounts of H₂. It is a typical low-heating-value gaseous fuel, with a lower heating value of $\sim 3700 \text{ kJ Nm}^{-3}$. While the COG dominantly contains H₂, CH₄, CO, CO₂, and N₂, with trace amounts of heavier hydrocarbon fuel, such as C₂H₂. The lower heating value of COG is $\sim 16\,200 \text{ kJ Nm}^{-3}$. China is the world's largest producer and consumer of iron and steel. Iron and steel producing are very energy-intensive manufacturing processes, producing large quantities of BFG and COG as byproducts. The use of these gaseous fuels can reduce the requirements for external fuels and the emissions of waste gas and CO₂,^{1,2} therefore, it is greatly important to recover and reuse these gaseous fuels.

Multifuel combustion is usually used to improve the economic performance by increasing the fuel flexibility, improving combustion behavior, mitigating operation problems, and decreasing gaseous pollutant emissions. The subject has been discussed in some studies,^{1–9} in which most of them focused on two-fuel combustion systems. Among the existing use methods for using BFG and COG, co-firing BFG and/or COG with pulverized coal in boilers is the most common method.^{3–6} It is flexible in boiler operating when the parameters of the BFG and/or COG stream are unstable, because the pulverized-coal feed rate can be increased to ensure the boiler load when the flow rate of BFG and/or COG decreases. COG is also able to serve as a reburning fuel for NO reduction in the power plant. Reburning technology

combined with overfire air (OFA) can reduce NO emission by $\sim 56\%$ in a 350 MW tangentially fired utility boiler using COG as the reburning fuel.⁵

When co-firing BFG with pulverized coal in a utility boiler, the main problem is that, with increasing the BFG flow rate, the carbon content in fly ash obviously rises, decreasing the pulverized-coal burnout.^{4,6} Therefore, the proper BFG flow rate is important to improve the boiler performance. Because of the more complex and high-coupled characteristics of flow, combustion, heat transfer, and NO emission in the three-fuel combustion system, such as co-firing pulverized coal with BFG and COG, it is critical to master more detailed information on the combustion process and control the flow rate of BFG and/or COG properly for improving the economic performance. Up to now, only Huang et al.¹⁰ carried out experimental detection using a temperature measuring system for the three-fuel combustion of coal, BFG, and COG in a utility boiler. However, it is difficult from the limited experimental data to exhibit more detail on the combustion process in the furnace and the effects of changing the flow rate of BFG and/or COG on the performance of the three-fuel boiler.

A numerical method, being able to reveal more detail, has been widely applied to investigate the combustion processes in different industrial combustors.^{11–26} Much numerical research

Special Issue: 2011 Sino-Australian Symposium on Advanced Coal and Biomass Utilisation Technologies

Received: July 31, 2011

Revised: November 15, 2011

Published: November 15, 2011

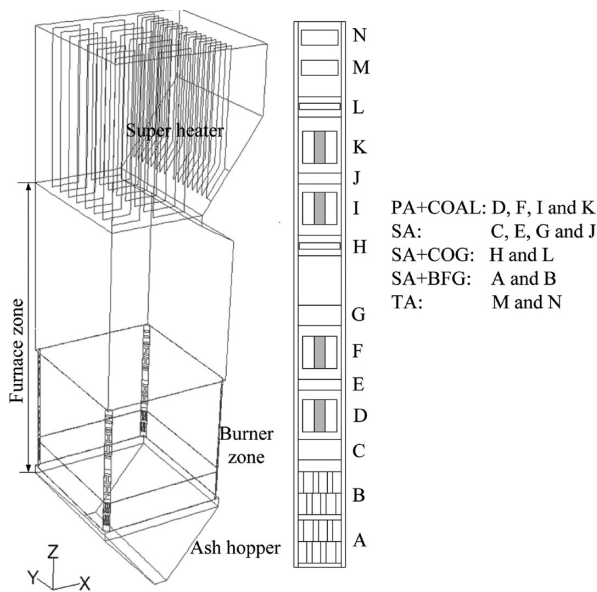


Figure 1. Schematic diagram of the furnace and burner nozzle arrangement at each corner.

has been conducted for single-fuel combustions, such as the conventional pulverized-coal combustion,^{11–16} biomass combustion,^{17,18} and oxy-fuel combustion.^{19,20} Several numerical studies have been performed for two-fuel combustion systems, such as two different coals,^{21,22} coal/biomass,²³ and coal/gaseous fuel.^{24,25} For a two-fuel system, both two-mixture-fraction^{21–24} and eddy-dissipation models²⁵ are suitable to model the gas-phase combustion. However, to the knowledge of the authors, no numerical study has been reported thus far on the three-fuel combustion system co-firing pulverized coal with BFG and COG in a utility boiler. Furthermore, the two-mixture-fraction model cannot be used to simulate the gas-phase combustion of a three-fuel system.

Therefore, it is the objective of this study to carry out numerical simulations on the combustion performance of a 200 MW tangentially fired utility boiler co-firing pulverized coal with BFG and COG. It was the first time to perform the numerical simulation of the three-fuel combustion in a utility boiler using the eddy-dissipation model to simulate the turbulent gas-phase reaction. The mesh and models adopted were validated by a mesh-independent test, an iteration convergence judgment, and a comparison of the simulated and experimental results. The co-combustion characteristics analysis was presented, and the effects of the flow rates of BFG and COG on the combustion performance of the boiler were investigated in detail.

2. METHODOLOGY

2.1. Boiler for Case Study. The case study boiler is a 200 MW tangentially fired utility boiler co-firing pulverized coal with BFG and COG. The furnace is 10.80, 11.92, and 44.60 m in depth, width, and height, respectively. Two sets of storage pulverized-coal preparation systems are used. At each corner, there are 16 burner nozzles, made up of four primary air (PA) nozzles, six secondary air (SA) nozzles, two tertiary air (TA) nozzles, two BFG nozzles, and two COG nozzles. The TA is injected into the furnace with a contrary tangent direction to the PA and SA. The contrary tangent angle is 10°. The BFG nozzles are located at the lowest position of the burner zone. The COG nozzles are

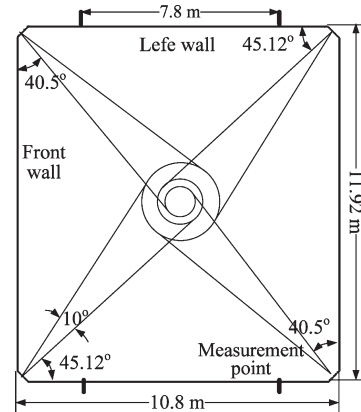


Figure 2. Schematic diagram of the furnace cross-section and measurement positions of the flame measuring system.

installed inside the H- and L-layer SA nozzles. There are a total of three groups of superheaters installed in the upper furnace. The schematic of the boiler furnace, burner nozzle configuration, and combustion system are shown in Figures 1 and 2. There are some observing ports on the water-cooled walls along the furnace height. The velocity and temperature of PA, SA, and TA are 24 m/s and 560 K, 42 m/s and 615 K, and 50 m/s and 350 K, respectively. The maximum flow rates of BFG and COG are 250 000 and 24 000 Nm³ h⁻¹.

2.2. Numerical Simulations. The numerical simulations were conducted on the basis of a computational fluid dynamics (CFD) code, known as Fluent 6.3.26. The combustion processes in the furnace include turbulent flow, pulverized-coal particle transport and combustion, gas-phase reaction, and radiative heat transfer. The calculation procedures include numerical solutions of the time-averaged conservation equations for the gas phase using the Eulerian description and the particle phase using the Lagrangian description. The turbulent flow was simulated by the standard $k-\varepsilon$ model. The stochastic particle trajectory model, which considers the effects of turbulence flow, was used to simulate the flow of the pulverized-coal particles in the furnace. The P1 method was used to simulate radiative heat transfer in the furnace. The heat absorption coefficient of combustion gases was calculated using the weighted sum of gray gases (WSGG) method. The particle emissivity, reflectivity, and scattering effects were included in the calculation of heat transfer. The pulverized coal combustion process can be divided into devolatilization and char combustion. The volatile yield rate was calculated using a single-rate kinetic devolatilization model, which assumes that the rate of devolatilization is dependent upon the amount of volatiles remaining in the particle via a first-order reaction. The total volatile yield was predicted using the chemical percolation devolatilization (CPD) model.²⁷ Char particle combustion was calculated by a kinetic and diffusion model.

Turbulent gas-phase combustion can be modeled using either the non-premixed combustion model or the species transport model. The non-premixed combustion model uses a modeling approach that solves transport equations for one or two conserved scalars, the mixture fractions. The concentrations of multiple species included in the problem definition will be derived from the predicted mixture fraction distribution. At present, no more than two mixture fractions can be solved, which are used to separately track the combustion processes of two fuels to reveal the effect of two fuels on the chemical reactions in local zones of the furnace. Therefore, a two-mixture-fraction model can only be used for a two-fuel combustion system. The species transport model directly solves transport equations for all species included in the problem definition. It can be used for the combustion system of more than two fuels. For the three-fuel combustion system in this study, the

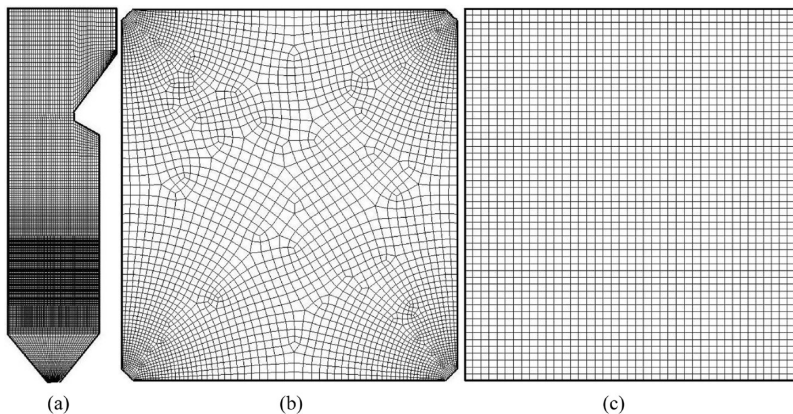


Figure 3. Mesh systems for different cross-sections: (a) $y = 5.96$ m, (b) $z = 10.4$ m, and (c) $z = 22.3$ m.

eddy-dissipation model was used to model the gas-phase turbulence combustion for the volatile matter produced from pulverized coal, BFG, and COG. The eddy-dissipation model assumes that the chemical reaction is fast relative to the transport processes in the flow.²⁸ When the volatile matter or other combustible components and oxygen are mixed at the molecular level, the reaction and formation of products take place instantaneously. The reaction paths of the volatile matter are represented by eqs 1 and 2, with α , β , and γ equal to 2.056, 1.136, and 2.232 for the used coal, respectively. The reaction paths of BFG are represented by eqs 2 and 3. The reaction paths of COG are represented by eqs 2, 3, and 4. More detailed descriptions of these models can be found in the literature.^{28,29}



NO_x simulation mainly considers the formation of thermal NO and fuel NO. Thermal NO is generated from the oxidation of N_2 in the combustion air. The formation of thermal NO is determined by a set of strongly temperature-dependent chemical reactions. The thermal NO was simulated using a simple combined kinetic rate expression for the classical Zeldovich mechanism.³⁰ The partial equilibrium approach for both atomic oxygen and hydroxyl radical was adopted. For the fuel NO modeling, the global models proposed by De Soete³¹ are considered as the fuel NO mechanism. It is assumed that the fuel-bound nitrogen of the coal is distributed between the volatile and the char. The nitrogen in the volatile evolves as HCN or NH_3 intermediates, and the nitrogen in the char converts to NO directly. The CPD model with the prediction of nitrogen release^{27,32} was adopted to predict the mass fraction of the nitrogen release in the volatile and the percentage of the nitrogen in the volatile evolved as the HCN intermediate. The mass fractions of volatile and char nitrogen are 0.266 and 0.734, respectively. The conversion fraction of char nitrogen is taken as 0.8.

A reburning model was included in the NO calculation because COG is a hydrocarbon-containing fuel with CH_4 . In the reburning reactions, the following three reactions are the most important reactions of NO reduction by CH radicals:³³



The hydrocarbon radicals involved in the above reactions are formed from the following elementary reactions:³³



The partial equilibrium approach³⁴ was applied to calculate the concentrations of important radicals. The reburning fuel was an equivalent of CH_3 approximately considering the C/H ratio of the fuel itself.²⁹

Because the concentration of NO is very small compared to the concentrations of other main species in coal combustion, the NO transport equation is commonly solved for a given combustion flow-field solution. The NO model is, therefore, typically employed with a post-processing method. The turbulent mixing process results in temporal fluctuations in the temperature and species concentration that will influence the characteristics of the flame. Temperature and composition fluctuations must be taken into account for the mean NO formation rate. In this study, an assumed shape of the probability density function (β PDF) was used to account for the temperature and oxygen species fluctuations on the NO formation in turbulent flows.^{16,24,28,29}

A partition meshing method was adopted to achieve a high-quality mesh with hexahedral grids. A mesh system with the mesh line being consistent with the flow direction in the near burner zone was established to decrease the pseudo-diffusion error. To obtain more accurate results, it is necessary to refine the meshes in the regions where the variables change very intensively, such as the surrounding regions of burner nozzles. Therefore, the meshes were refined in the zones near the burner nozzles. Two interfaces were used to keep the burner zone connected with the other zone of the furnace. The meshes in the burner zone were changed to conducted mesh-independent tests. The mesh system adopted is shown in Figure 3. The PISTO method was used to consider the interaction between gas and particle phases. The SIMPLE algorithm of pressure correction was applied to consider the coupling of velocity and pressure fields. Using the first-order finite difference method, the conservation equations of the gas phase were solved with successive under-relaxation iterations until the solution satisfied pre-specified residuals, which were set to 1×10^{-6} for the iterations of energy, radiation, and NO equations and 1×10^{-4} for other equations.

The simulations were carried out for a total of nine cases. The properties of the coal, BFG, and COG used in the simulations and

experiments are shown in Table 1. The multifuel combustions were conducted in cases 1–8, and the single-fuel combustion with only pulverized coal was also conducted in case 9 for the purpose of comparison. The operating conditions of all nine cases are listed in Table 2. The studied boiler is usually operated at the load of less than 180 MW. Therefore, the loads for all cases are not more than 180 MW. To prevent overheating or severe wear of the heat-exchanging surfaces, a low oxygen concentration in flue gas at the furnace exit was used at the 180 MW load. The wall function method and temperature wall were employed for the velocity and thermal boundary conditions, respectively. The wall temperature and emissivity were 698 K and 0.6. The size distribution of the pulverized coal particles obeys the Rosin–Rammmer algorithm, with an average diameter of 65 μm and a spread parameter of 1.5. A total of 90% of the pulverized coal was injected into the furnace from the PA nozzles, and the remaining 10% was injected into the furnace from the TA nozzles. BFG and COG were injected into the furnace from the BFG and COG nozzles. The kinetics parameters, such as the pre-exponential factor and activation energy of coal devolatilization, are 492 000 s^{-1} and 74 000 kJ/kmol , while those for char combustion are 0.0018 $\text{kg m}^{-2} \text{s}^{-1} \text{Pa}^{-1}$ and 83 700 kJ/kmol .

Table 1. Fuel Properties

item	value	item	value
coal proximate analysis (wt %, as air-dried)		fuel gas species (vol %)	BOG COG
volatile matter	12.8	carbon monoxide	26.6 7.9
moisture	1.58	hydrogen	3.5 59.0
ash	35.74	methane	0 21.6
fixed carbon	49.88	C_2H_2	0 2.2
coal ultimate analysis (wt %, as air-dried)		carbon dioxide	20.6 2.6
carbon	54.62	oxygen	0.4 0.8
hydrogen	2.799	nitrogen	49.0 5.9
oxygen	5.519	lower heating value (kJ Nm^{-3})	3730 16210
nitrogen	0.883		
sulfur	0.486		
lower heating value (kJ/kg)	19100		

Table 2. Simulation and Experimental Cases

case	load (MW)	air flow rate (kg/s)	coal feed rate ^a (kg/s)	BOG flow rate ^b ($\text{Nm}^3 \text{h}^{-1}$)	COG flow rate ^c ($\text{Nm}^3 \text{h}^{-1}$)	ratio of BFG heat input (%)	ratio of COG heat input (%)
1	168	154.53	12.50	200000	9000	37.10	8.38
2	150	155.53	11.11	200000	12000	38.35	11.55
3	135	159.02	9.17	200000	15000	40.74	15.33
4	180	140.51	17.36	0	5000	0	5.79
5	180	143.45	16.57	50000	5000	10.76	5.40
6	180	149.53	15.80	100000	5000	20.13	5.05
7	180	147.58	16.44	100000	0	20.55	0
8	180	149.16	14.80	100000	10000	20.07	10.07
9	180	140.52	18.20	0	0	0	0

^a A total of 11 (D, F, and I layers), 10 (D, F, and I layers), and 8 (D and F layers) PA and pulverized-coal burners were in service for cases 1, 2, and 3, respectively. A total of 12 (D, F, and I layers) PA and pulverized-coal burners were in service for cases 4–9. ^b All 8 (A and B layers) BFG burners were in service for cases 1–3. A total of 0 BFG burner were in service for case 4. A total of 2 (B layer) BFG burners were in service for case 5. A total of 4 (B layer) BFG burners were in service for cases 6–8. ^c A total of 3 (H layers), 4 (H layers), and 5 (H and L layers) COG burners were in service for cases 1, 2, and 3, respectively. A total of 2 (H layers) COG burners were in service for cases 4–6. A total of 0 COG burners were in service for case 7. A total of 4 (H layers) COG burners were in service for case 8.

2.3. Full-Scale Experimental Measurements. Combustion experimental measurements were conducted under the different conditions of the eight cases. A carefully calibrated portable flame temperature measuring system using a visible flame image processing technique was employed to measure the flame temperatures along the furnace height. The measuring system includes a flame image detector, a video collecting card, a notebook computer, and the image processing software. It can take flame images and calculate the image temperatures in a very short time. The range of measured temperatures is from 500 to 2000 °C. The radiation images of red (R) and green (G) are obtained from the color flame image and are assumed directly proportional to the approximately monochromatic radiations at their central wavelengths of $\lambda_r = 610.8 \text{ nm}$ and $\lambda_g = 510.8 \text{ nm}$, respectively, after a careful test of the charge coupled device (CCD) camera used in the measurements. The flame temperature measurement is based on Planck's radiation law for blackbody radiation. A blackbody furnace with the temperature range from 1000 to 2000 K (with temperature errors within $\pm 5 \text{ K}$) is used to carefully calibrate the flame image detector. The flame image temperature can be computed by the two-color method. The measuring system and method were described in more detail by Wang et al.³⁵ The combustion was maintained to be stable during the measurements. At each cross-section, the system was used to measure the temperatures through the four observing ports in turn (see Figure 2). The average temperature was then calculated to represent the temperature level at this cross-section.¹⁴

Some performance parameters, such as the carbon content in fly ash, the oxygen concentration and NO emission in flue gas, and the exhaust gas temperature, were measured. A MSI EURO-type flue gas analyzer was used to measure the components of flue gas. The flue gas and fly ash samplings were conducted at the entrance of the air preheater. The exhaust gas temperature was measured at the air preheater exit. Coal sampling was carried out at the coal hopper exits. Pulverized coal sampling was carried out using the sampling equipment installed on the pipes of primary air and pulverized coal mixture. Bottom ash was also sampled.

3. RESULTS AND DISCUSSION

3.1. Validation of the Numerical Simulations. To obtain a confidence for the established mesh and adopted models in the present study, the numerical simulations are validated by mesh-independent tests, iteration convergence judgment, and the comparisons between the calculated and experimental results.

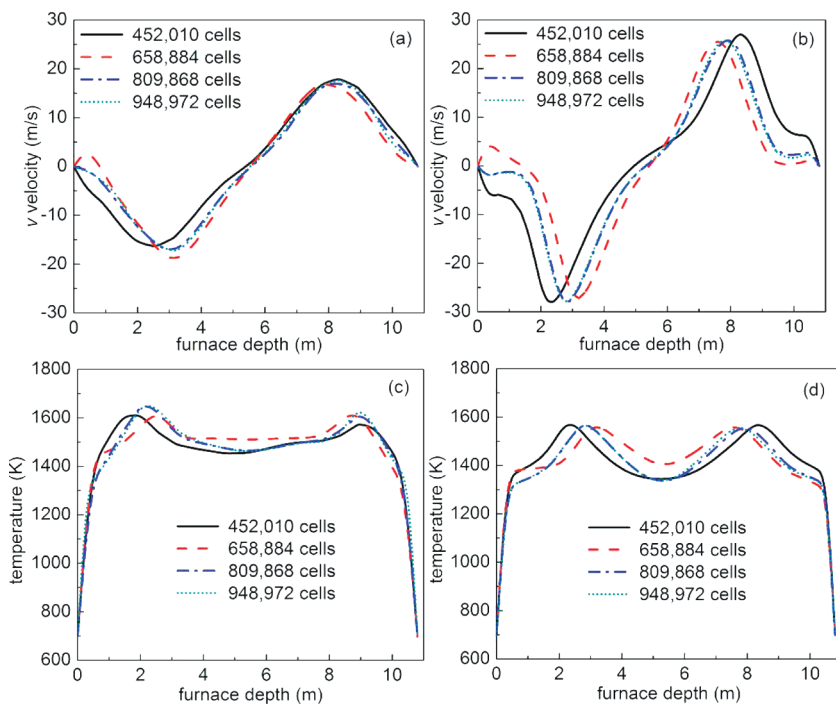


Figure 4. Mesh independence test: (a) gas velocity v and (c) gas temperature along line 1 ($x = 0$ – 10.8 m, $y = 5.96$ m, and $z = 10.34$ m in the D-layer PA and coal burner cross-section) and (b) gas velocity v and (d) gas temperature along line 2 ($x = 0$ – 10.8 m, $y = 5.96$ m, and $z = 7.77$ m in the B-layer BFG burner cross-section).

Table 3. Converged Residuals of Cases 1–3

item	continuity ($\times 10^{-6}$)	V_x ($\times 10^{-5}$)	V_y ($\times 10^{-5}$)	V_z ($\times 10^{-5}$)	k ($\times 10^{-5}$)	ε ($\times 10^{-5}$)	energy ($\times 10^{-7}$)	P1 ($\times 10^{-7}$)
case 1	4.3924	1.1818	1.2345	1.0943	1.0617	1.3815	6.8894	9.8973
case 2	4.4814	1.2510	1.3002	1.1022	1.3909	1.6849	8.4349	9.9469
case 3	6.8702	1.2754	1.3614	1.0897	1.4381	1.9533	9.529	9.9149
item	H_2O ($\times 10^{-6}$)	O_2 ($\times 10^{-6}$)	CO ($\times 10^{-6}$)	CO_2 ($\times 10^{-6}$)	H_2 ($\times 10^{-6}$)	CH_4 ($\times 10^{-5}$)	lv-vol ($\times 10^{-5}$)	
case 1	1.9760	4.9935	3.1461	1.1309	8.0443	1.2886	1.1323	
case 2	2.0682	4.7575	3.5395	1.1858	9.9594	1.4852	1.2496	
case 3	2.3302	5.2384	3.997	1.0395	9.0395	1.4703	1.3506	

The comparisons are conducted for the average temperature along the furnace height and some parameters at the furnace exit, such as the carbon content in fly ash, the burnout degree of pulverized coal, and the oxygen concentration and NO emission in flue gas.

Grid-independent tests were first conducted for case 1. Four mesh systems with 452 010, 658 884, 809 868, and 948 972 cells were used. Mesh independence was checked by comparing the gas-phase horizontal velocity component v and the gas temperature along line 1 ($x = 0$ – 10.8 m, $y = 5.96$ m, and $z = 10.34$ m in the D-layer PA and coal burner cross-section) and along line 2 ($x = 0$ – 10.8 m, $y = 5.96$ m, and $z = 7.77$ m in the B-layer BFG burner cross-section) in the furnace (see Figure 4). Panels a and b and c and d of Figure 4 show the comparisons of gas velocity v and temperature profiles of lines 1 and 2 for the four mesh systems, respectively. The results are similar for the meshes with 809 868 and 948 972 cells. Therefore, the mesh system of 809 868 cells was adopted for other cases in the present study.

The converged solutions can be obtained after 5141, 4343, and 5989 iterations for cases 1–3, and the converged residuals are

present in Table 3. These indicate good convergence for the simulations. The calculated average temperature profiles are compared to those measured along the furnace height for cases 1–3. Figure 5 indicates that the calculated temperatures agree well with the measured values, with the maximum errors of 4.52, 5.46, and 5.24% at 168, 150, and 135 MW loads, respectively. The comparisons of the calculated and measured values for the carbon content in fly ash, the burnout degree of pulverized coal, and the oxygen concentration and NO emission in flue gas at the furnace exit are shown in Table 4. The calculated results show good agreement with those measured with the maximum error less than 10% for all of these parameters. The simulated results can properly reveal the combustion and NO emission characteristics for the boiler in this study. All of the above data (Figures 4 and 5 and Tables 3 and 4) offer a solid validation for the numerical simulations and indicate that the mesh and models adopted in the present study are suitable for investigating the three-fuel combustion of the boiler.

3.2. Co-combustion Characteristics Analysis. Figure 6 presents the velocity fields of central cross-sections of the BFG, pulverized

coal, and COG nozzles in case 1. It can be seen that good tangential circles form in the central zone of these cross-sections, which indicates a good flow field inside the furnace. Because of the bigger momentum and stronger rigidity of the BFG and auxiliary SA mixture flow, the tangential circle of the BFG cross-section is less than those of the pulverized-coal and COG cross-sections. Figure 7 presents the temperature distributions of three cross-sections. The

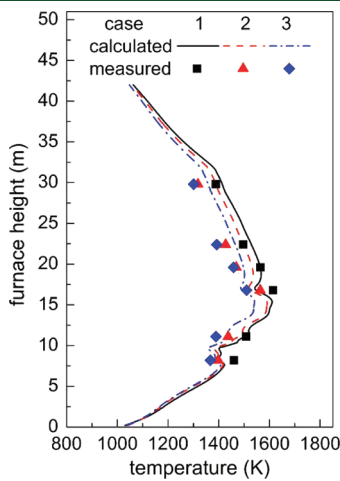


Figure 5. Comparison of the calculated and measured average temperature profiles along the furnace height.

Table 4. Comparison of the Calculated and Measured Results in Cases 1–3

case number	1	2	3	
average residence time of coal particles (s)	5.99	5.91	5.78	
carbon content in fly ash (%)	calculated measured error ^a	8.29 7.61 8.93	6 5.03 9	4.85 −3.58
burnout degree of pulverized coal (%)	calculated measured error ^a	92.98 94.6 −1.71	94.56 95.56 −1.05	96.05 96.11 −0.06
NO emission (ppm, 6% O ₂)	calculated measured error ^a	254 281 −9.61	230 231 −0.43	207 189 9.52
O ₂ at the exit (vol %)	calculated measured error ^a	2.18 2.04 6.86	2.68 2.63 1.91	3.7 3.43 7.87

^a Error = (calculated – measured)/measured × 100.

temperature of the BFG cross-section is relatively low, with a maximum value of 1571 K, because of the low heating value of BFG, while the temperatures of the cross-sections of pulverized coal and COG are much higher, with the maximum values of 1765 and 1779 K. The high-temperature zone of the COG cross-section is larger than that of the pulverized coal cross-section.

The comparison of the temperature variances along the central lines of the BFG, pulverized coal, and COG nozzles is shown in Figure 9. The temperatures for the BFG and COG nozzles in the early stage rise up more rapidly than that for the pulverized coal nozzle. With the position of 1000 K on the nozzle central line defined as the ignition point,³⁶ the ignition distance is quantified. It can be found that the ignition distance of the pulverized coal mixture is longer than those of the BFG and COG. The combustion process of pulverized coal includes devolatilization and char combustion. After the pulverized-coal particles are injected into the furnace, they absorb the convective and radiative heat. The particle temperatures rise up, and the particles start to devolatilize. When the local volatile matter concentration reaches a certain value, the volatile matter starts to combust in the gas phase and then the PA and pulverized-coal mixture is ignited. This process is slower than those of BFG and COG because the gaseous fuels mix with oxygen at the molecular level more rapidly. Because of the interval layout of the BFG and auxiliary SA nozzles (see Figure 1), the combustible components of BFG and oxygen mix more rapidly; therefore, the ignition distance of BFG is shorter than that of COG. However, after the COG has been ignited, the temperature rises faster because of the higher heating value.

Figure 8 presents the NO concentration distributions of central cross-sections of the BFG, pulverized coal, and COG nozzles. For the pulverized-coal cross-section, NO is mainly concentrated in the zone where the combustion is very intense and the temperature is relatively high (see panel b of Figures 8 and 7). The maximum NO concentration is 512 ppm. NO distributes across almost the whole COG cross-section because of the effects of turbulent flow convection and diffusion. Because COG contains the components such as CH₄, H₂, and CO and is a reburning fuel for NO reduction, part of NO formed is reduced at the COG cross-section. The maximum NO concentration therefore decreases, and the maximum value is 447 ppm. In comparison to the NO concentrations in the pulverized-coal and COG cross-sections, that in the BFG cross-section is much lower, with a maximum value of 57 ppm. The reason is that the temperature is relatively low and little pulverized-coal particles burn here because of the strong carrying capacity of the BFG and SA mixture flow.

3.3. Effects of Increasing the BFG Flow Rate. Figure 10a presents the average temperature profiles along the furnace height,

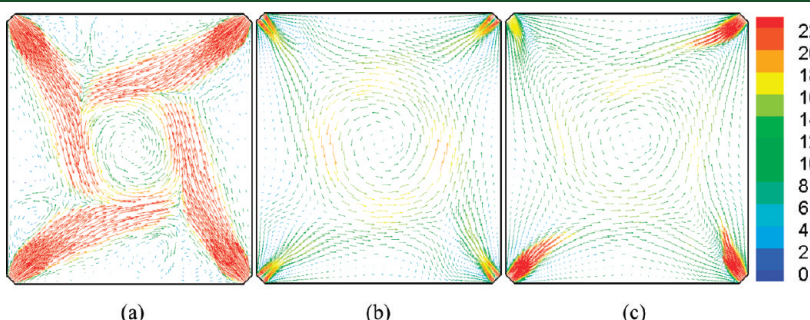


Figure 6. Velocity fields of central cross-sections of (a) BFG, (b) pulverized coal, and (c) COG nozzles in case 1 (unit: m/s).

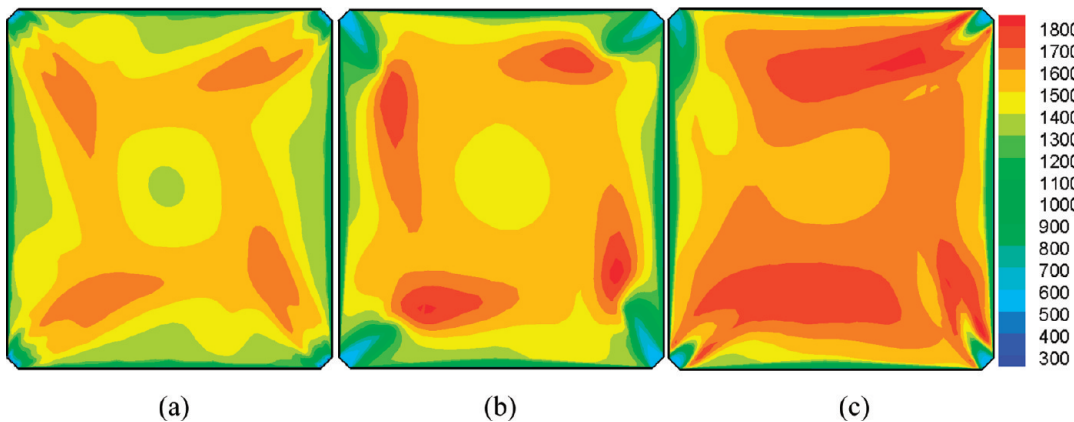


Figure 7. Temperature distributions of central cross-sections of (a) BFG, (b) pulverized coal, and (c) COG nozzles in case 1 (unit: K).

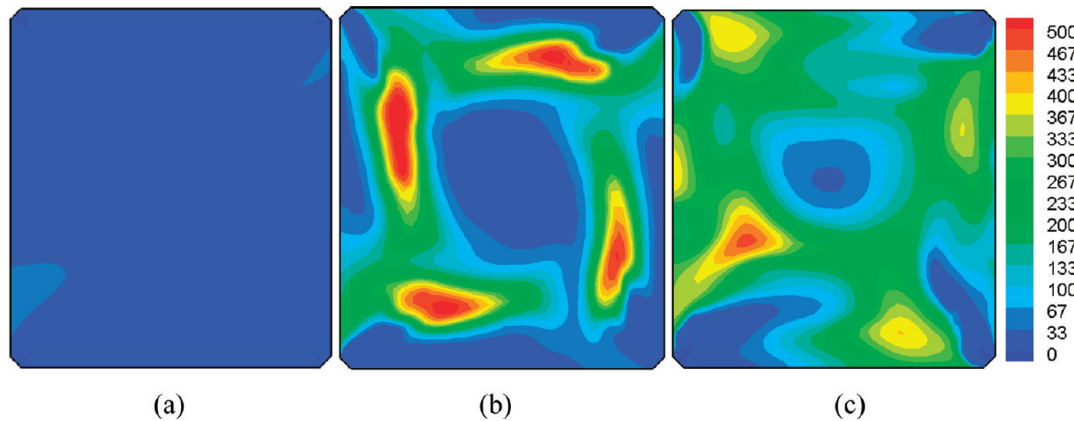


Figure 8. NO concentration distributions of central cross-sections of (a) BFG, (b) pulverized coal, and (c) COG nozzles in case 1 (unit: ppm).

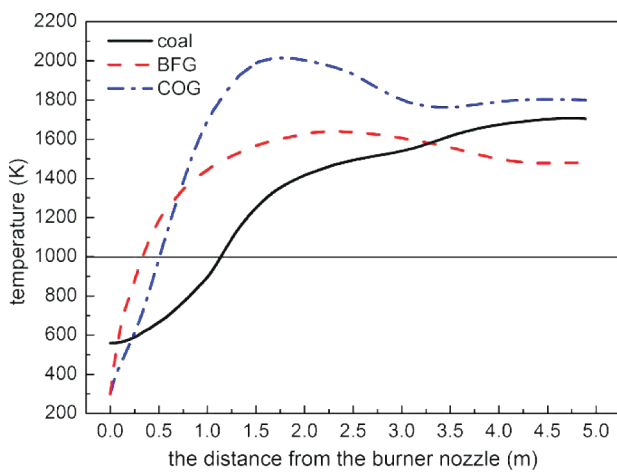


Figure 9. Comparison of variation of the temperature along the central lines of the BFG, pulverized coal, and COG nozzles in case 1.

and panels a–c of Figure 11 show the high-temperature zones of 1750 K in the furnace for cases 4–6. Both the simulated and experimental results show that, with increasing the BFG flow rate, the in-furnace temperature decreases and the high-temperature zone reduces gradually. As shown in Table 5, increasing the BFG flow rates of 10 and 20% heat input

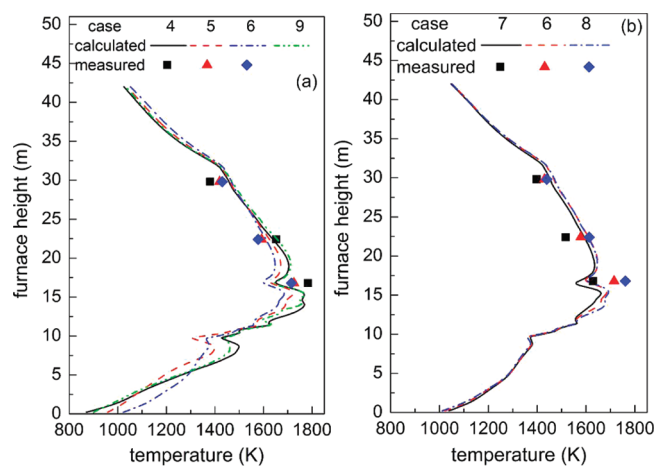


Figure 10. Comparison of the average temperature profiles along the furnace height: (a) changing the BFG flow rate and (b) changing the COG flow rate.

decreases about 33 and 58 K in the average temperature of the furnace zone (see Figure 1).

The comparison of variation of the temperature along the central line of the PA nozzle is shown in Figure 12a. As the BFG flow rate increases, the temperature in the early stage rises more

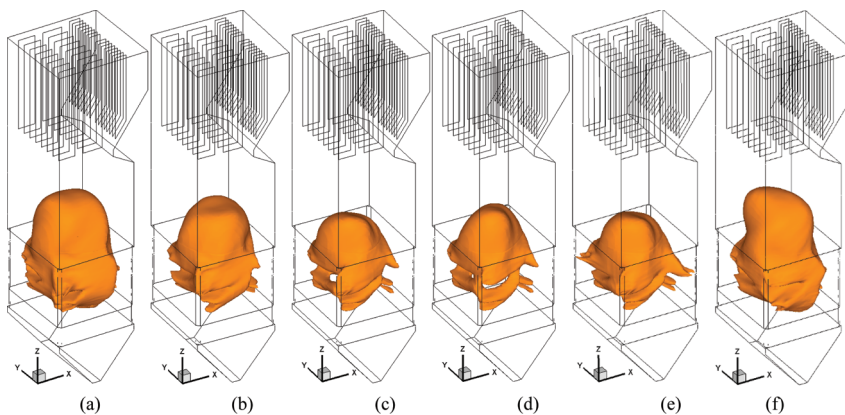


Figure 11. Isothermal surface temperature of 1750 K for cases (a) 4, (b) 5, (c) 6, (d) 7, (e) 8, and (f) 9.

Table 5. Calculated and Measured Results in Cases 4–9

case number	4	5	6	7	8	9
calculated average residence time of coal particles (s)	9.32	8.25	6.94	6.89	6.96	9.50
calculated carbon content in the fly ash (%)	2.46	3.76	5.01	5.48	4.66	2.50
calculated burnout degree of pulverized coal (%)	97.55	96.97	95.43	95.02	95.73	97.52
calculated O ₂ concentration at the exit (vol %)	2.07	1.92	2.02	1.93	2.02	2.01
calculated flue gas rate (kg/s)	151.80	168.42	187.88	188.18	186.03	151.78
calculated average temperature at the nose (K)	1401	1414	1428	1436	1426	1417
calculated average temperature of the furnace zone (K)	1569	1536	1511	1507	1514	1554
calculated NO emission at the exit (ppm, 6% O ₂)	thermal NO total NO	86 386	37 369	25 344	13 427	30 315
measured exhaust gas temperature (K)	140	146	153	155	150	147
boiler thermal efficiency (%)	91.19	89.68	88.80	87.32	89.82	90.1

slowly and the ignition distance increases. Because of the decrease of the in-furnace temperature, the convective and radiative heat absorbed by the PA and pulverized-coal mixture reduces, delaying the ignition of the PA and pulverized coal mixture. This will delay the burnout process of the pulverized coal.

The statistic parameters at the furnace exit are listed in Table 5. The oxygen concentrations in flue gas at the furnace exit are about 2.0% for cases 4–8. It can be seen that, with increasing the BFG flow rate, the carbon content of fly ash increases and, consequently, the burnout degree of pulverized coal decreases. The reasons come from two points. First, the decrease of the in-furnace temperature delays the ignition and burnout processes of pulverized coal and also lowers the pulverized-coal combustion rate. Second, the residence time of pulverized-coal particles in the furnace was decreased with increasing the flow rate and velocity of flue gas as a result of increasing the BFG flow rate.

As shown in Table 5, the average temperature at the furnace nose rises with the increase of the BFG flow rate. It can be seen from panels a–c of Figure 13 that, with increasing the BFG flow rate, the high-heat-flux zone reduces and moves upward and the maximum heat flux also decreases. These indicate that the flame center rises and the heat absorbed by the water-cooled walls reduces, increasing the average temperature at the furnace nose. It will bring a negative effect on the heat-transfer characteristics of the heat-exchanging surfaces. The heat loss because of exhaust gases are increased because of the increase of the exhaust gas temperature (see Table 5). The boiler thermal efficiency decreases with the increase of the BFG flow rate.

Figure 14a presents the average CO concentration profiles along the furnace height for changing the BFG flow rate. The average CO concentration at the BFG burner zone is higher than those at coal and COG burner zones because the mole fraction of CO in BFG is high, with the value of 0.266. However, in case 4 (without BFG), the average CO concentration at the BFG burner zone is very low because of no BFG injection. With increasing the BFG flow rate, the average CO concentration is largely increased at the BFG burner zone.

Figure 15a presents the average NO concentration profiles along the furnace height. In case 4 (without BFG), the maximum NO concentration is located in the central burner zone, where the combustion is very intense. The NO concentration is also high in the ash hopper because a lot of pulverized-coal particles from the PA nozzles go through the SA turbulent flow, move into the ash hopper, and continue to combust intensively. As the BFG flow rate increases, the decrease of the high-temperature zone reduces the formation of thermal NO (see Table 5) and the decrease of the feed rate and burnout degree of pulverized coal produce less fuel NO, decreasing the total NO concentration. Because more BFG together with auxiliary SA is injected into the furnace from the B-layer nozzle, the turbulent flow carrying capacity is enhanced and the number of pulverized-coal particles moving into the ash hopper is reduced, decreasing the NO concentration in the ash hopper significantly. Also, some formed NO can be reduced because of the reduction effect of CO. As shown in Table 5, the NO emission at the furnace exit reduces with increasing the BFG flow rate.

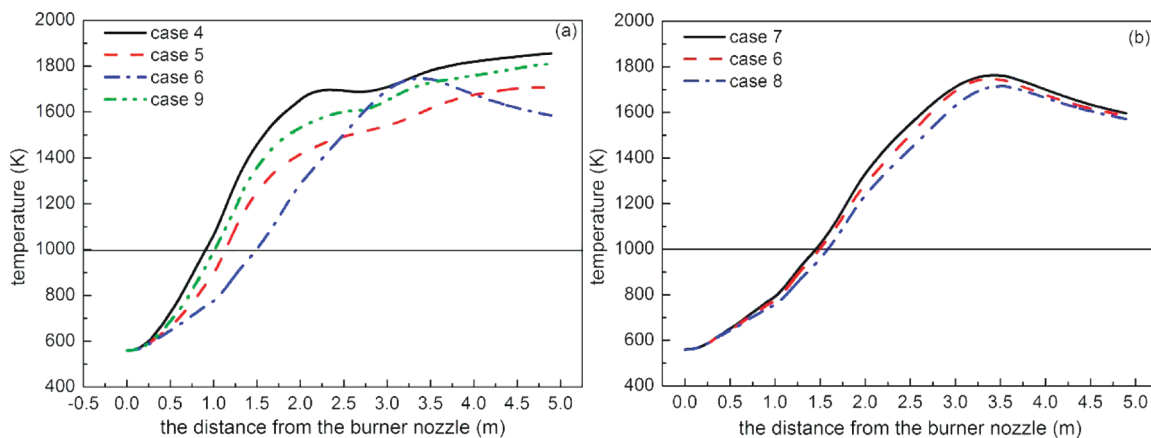


Figure 12. Comparisons of variation of the temperature along the central line of the PA nozzle: (a) changing the BFG flow rate and (b) changing the COG flow rate.

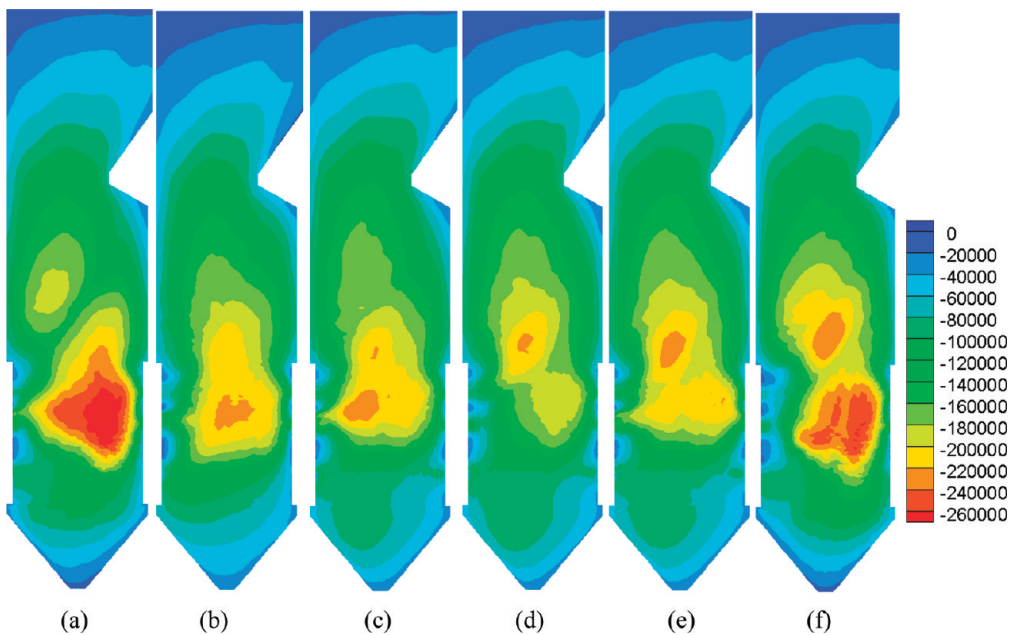


Figure 13. Heat flux distributions on the right water-cooled walls for cases (a) 4, (b) 5, (c) 6, (d) 7, (e) 8, and (f) 9 (unit: W/m^2 , and negative stands for absorbing heat).

3.4. Effects of Increasing the COG Flow Rate. Figure 10b presents the average temperature profiles along the furnace height, and panels c–e of Figure 11 show the high-temperature zones of 1750 K for cases 6–8. With increasing the COG flow rate, both the in-furnace temperature and the high-temperature zone increase. Increasing the COG flow rates of 5 and 10% heat input increases the average temperatures of the furnace zone by about 3 and 7 K (see Table 5). The comparison of variation of the temperature along the central line of the PA nozzle is shown in Figure 12b. As the COG flow rate increases, the ignition distance of the PA and pulverized-coal mixture increases slightly. This is mainly caused by the reduction of the in-furnace temperature in the D-layer nozzle zone because of the decrease of the coal feeding rate for PA nozzles.

As shown in Table 5, the carbon content of fly ash decreases and the burnout degree of pulverized coal increases with the increase of the COG flow rate. On one hand, the pulverized-coal

combustion rate increases because of the increase of the in-furnace temperature. On the other hand, both the flow rate and velocity of flue gas decrease (see Table 5), increasing the residence time of pulverized-coal particles in the furnace.

The average temperature at the furnace nose decreases slightly with the increase of the COG flow rate (see Table 5). As shown in panels c–e of Figure 13, with increasing the COG flow rate, the high-heat-flux zone enlarges and moves downward, indicating that the flame center shifts downward and the heat absorbed by the water-cooled walls increases. These are helpful for reducing the average temperature at the furnace nose and improving the heat-transfer characteristics of different heat-exchanging surfaces. The exhaust gas temperature decreases (see Table 5), decreasing the heat loss because of exhaust gases. The boiler thermal efficiency increases with the increase of the COG flow rate.

Figure 14b presents the average CO concentration profiles along the furnace height for changing the COG flow rate. It can

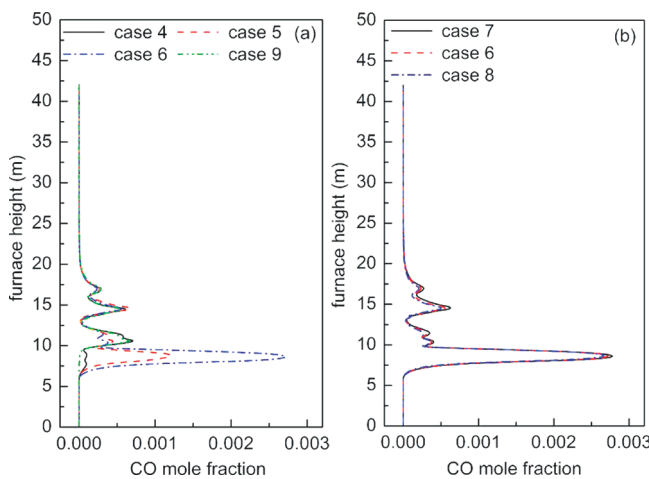


Figure 14. Comparisons of the average CO concentration profiles along the furnace height: (a) changing the BFG flow rate and (b) changing the COG flow rate.

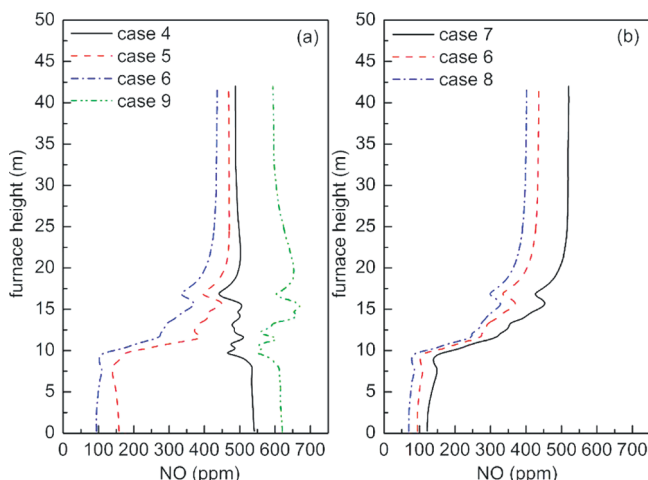


Figure 15. Comparisons of the average NO concentration profiles along the furnace height: (a) changing the BFG flow rate and (b) changing the COG flow rate.

be seen that increasing the COG flow rate has little effect on the average concentration profiles along the furnace height.

Figure 15b presents the average NO concentration profiles along the furnace height for changing the COG flow rate. With increasing the COG flow rate, the NO concentration decreases gradually. More of the NO formed is reduced, although the formation of thermal NO slightly increases because of the increase of the in-furnace temperature. Also, the less fuel NO forms with the lower coal feed rate. Because of the delay of the pulverized-coal ignition and burnout processes, the maximum NO concentration is located in the upper furnace zone. The NO concentration in case 7 is much higher than those of the other cases in the upper furnace because no COG is injected into the furnace. Because there are no special reburning and OFA nozzles for the studied boiler, only part of COG and BFG takes part in the reduction reactions with NO and the efficiency for NO reduction is much less than the reported data.⁵ As shown in Table 5, the NO emission at the furnace exit reduces with the increase of the COG flow rate.

3.5. Characteristics of Pulverized Coal Combustion. In comparison to the characteristics of co-firing pulverized coal with COG of 5.79% of the total heat input in case 4, the furnace temperature decreases with a decrease of 15 K in the average temperature of the furnace zone (Figure 10a and Table 5) and the high-temperature zone of 1750 K narrows and elongates (Figure 11f) when only pulverized coal was burned in the furnace. The reason is that the combustion rate and burnout time of pulverized coal are much slower and longer than those of COG. The high-heat-flux zone reduces, and the maximum heat flux also decreases (Figure 13f), indicating that the heat absorbed by the water-cooled walls reduces. This results in the increase of the average temperature at the furnace nose (Table 5). It will bring a negative effect on the heat-transfer characteristics of the heat-exchanging surfaces, decreasing the boiler thermal efficiency. Because of the decrease of the in-furnace temperature, the ignition distance of the PA and pulverized-coal mixture increases (Figure 12a). The carbon content of fly ash increases slightly, and consequently, the burnout degree of pulverized coal decreases slightly. This is mainly because the decrease of the in-furnace temperature lowers the pulverized-coal combustion rate and delays the burnout processes of pulverized coal, although the residence time of pulverized-coal particles has a little increase.

The maximum NO concentration is located in the upper PA and pulverized-coal burner zone (Figure 14a), where the combustion temperature is highest (Figure 10a). Because there is no NO reduction by COG and BFG, the NO concentration along the furnace height is higher and the NO emission at the exit increases (Table 5) compared to those for co-firing coal with COG and BFG.

As analyzed in sections 3.3 and 3.4, burning BFG brings negative effects on the ignition of primary air and pulverized-coal mixture, pulverized-coal burnout, and heat transfer in the furnace and, consequently, decreases the thermal efficiency (cases 5–8).

On the basis of the discussion above, co-firing pulverized coal with BFG of ~20% heat input and COG of ~10% heat input is an optimal operating condition at 180 MW load for the boiler in this study.

4. CONCLUSION

Numerical simulations were carried out to investigate the performance of a 200 MW multifuel tangentially fired utility boiler co-firing pulverized coal with BFG and COG. The eddy-dissipation model was used to calculate the combustion of the gas phase with the participation of multifuels in the simulations. The numerical simulations obtained a solid validation for the mesh and models adopted by mesh-independent tests, iteration convergence judgment, and the comparisons between the calculated and experimental results. The effects of the BFG and COG flow rates on the boiler performance were investigated under the same load of 180 MW.

With increasing the BFG flow rate, the in-furnace temperature decreases, the PA and pulverized coal mixture ignition delays, and the residence time of pulverized-coal particles shortens, decreasing the pulverized-coal burnout degree. The flue gas flow rate and exhaust gas temperature increase. Both the heat losses because of incomplete combustion of solid combustibles and exhaust gases increase, decreasing the boiler thermal efficiency. However, with increasing the COG flow rate, the pulverized-coal burnout degree is increased as a result of the increase of the

in-furnace temperature and residence time of the pulverized-coal particle. The flue gas flow rate and exhaust gas temperature decrease. Both the heat losses because of incomplete combustion of solid combustibles and exhaust gases decrease, increasing the boiler thermal efficiency. Increasing both the BFG and COG flow rates can reduce the NO emissions. Co-firing pulverized coal with BFG of about 20% heat input and COG of about 10% heat input is an optimal operating condition under the boiler load of 180 MW. The present study provides helpful information for understanding and optimizing the multifuel combustion of the boiler.

■ AUTHOR INFORMATION

Corresponding Author

*Telephone: +86-27-87557815. Fax: +86-27-87540249. E-mail: hczhou@mail.hust.edu.cn.

■ ACKNOWLEDGMENT

The authors gratefully acknowledge the financial support for this research from the National Natural Science Foundation of China (50806024, 51025622, and 51021065). The authors thank Prof. Hongwei Wu and Mr. Xiangpeng Gao for their help in improving the paper.

■ REFERENCES

- (1) Hou, S. S.; Chen, C. H.; Chang, C. Y.; Wu, C. W.; Ou, J. J.; Lin, T. H. *Energy Convers. Manage.* **2011**, *52*, 2758–2767.
- (2) Bojic, M.; Moudoukoutas, P. *Appl. Therm. Eng.* **2000**, *20*, 963–975.
- (3) Shieh, S. S.; Chang, Y. H.; Jang, S. S.; Ma, M. D.; Huang, T. S. *Fuel* **2010**, *89*, 1141–1149.
- (4) Ma, H. K.; Wu, F. S. *Int. Commun. Heat Mass Transfer* **1992**, *19*, 409–421.
- (5) Su, S.; Xiang, J.; Sun, L. S.; Hu, S.; Zhang, Z. X.; Zhu, J. M. *Fuel Process. Technol.* **2009**, *90*, 396–402.
- (6) Zhan, Z. G.; Chen, G. *Power Eng.* **2004**, *24*, 179–182 (in Chinese).
- (7) Gicquel, O.; Vervisch, L.; Joncquet, G.; Labegorre, B.; Darabiha, N. *Fuel* **2003**, *82*, 983–991.
- (8) Abbas, T.; Awais, M. M.; Lockwood, F. C. *Combust. Flame* **2003**, *132*, 305–318.
- (9) Gani, A.; Morishita, K.; Nishikawa, K.; Naruse, I. *Energy Fuels* **2005**, *19*, 1652–1659.
- (10) Huang, B. Y.; Luo, Z. X.; Fang, Q. Y.; Zhou, H. C. *J. Eng. Thermophys.* **2010**, *31*, 1065–1068 (in Chinese).
- (11) Zhou, H.; Mo, G. Y.; Si, D. B.; Cen, K. F. *Energy Fuels* **2011**, *25*, 2004–2012.
- (12) Ren, F.; Li, Z. Q.; Liu, G. K.; Chen, Z. C.; Zhu, Q. Y. *Energy Fuels* **2011**, *25*, 1457–1464.
- (13) Tian, Z. F.; Witt, P. J.; Schwarz, M. P.; Yang, W. *Energy Fuels* **2010**, *24*, 4971–4979.
- (14) Fang, Q. Y.; Wang, H. J.; Zhou, H. C. *Energy Fuels* **2010**, *24*, 4857–4865.
- (15) Vuthaluru, R.; Vuthaluru, H. B. *Fuel Process. Technol.* **2006**, *87*, 633–639.
- (16) Choi, C. R.; Kim, C. N. *Fuel* **2009**, *88*, 1720–1731.
- (17) Yin, C. G.; Rosendahl, L.; Kær, S. K. *Energy Fuels* **2008**, *22*, 1380–1390.
- (18) Ma, L.; Jones, J. M.; Pourkashanian, M. *Fuel* **2007**, *86*, 1959–1965.
- (19) Tiggese, K. D.; Klauke, F.; Berginsa, C. *Energy Procedia* **2009**, *1*, 549–556.
- (20) Toporov, D.; Bocian, P.; Heil, P. *Combust. Flame* **2006**, *155*, 605–618.
- (21) Shen, Y. S.; Guo, B. Y.; Yu, A. B.; Zulli, P. *Fuel* **2009**, *88*, 255–263.
- (22) Sheng, C. D.; Moghtaderi, B.; Gupta, R.; Wall, T. F. *Fuel* **2004**, *83*, 1543–1552.
- (23) Pallarés, J.; Gil, A.; Cortés, C.; Herce, C. *Fuel Process. Technol.* **2009**, *90*, 1207–1213.
- (24) Su, S.; Xiang, J.; Sun, X. X. *Energy Fuels* **2006**, *20*, 1434–1443.
- (25) Xu, G.; Zhou, W.; Swanson, L. W.; Moyeda, D. K.; Nguyen, Q. *J. Therm. Sci. Eng. Appl.* **2009**, *1*, 1–6.
- (26) Shi, Y.; Green, W. H.; Wong, H. W.; Oluwole, O. O. *Combust. Flame* **2011**, *158*, 836–847.
- (27) Genetti, D.; Fletcher, T. H. *Energy Fuels* **1999**, *13*, 1082–1091.
- (28) Smoot, L. D.; Smith, P. J. *Coal Combustion and Gasification*; Plenum Press: New York, 1989.
- (29) Fluent, Inc. *Fluent 6.3 User's Guide*; Fluent, Inc.: New York, 2006.
- (30) Hill, S. C.; Smoot, L. D. *Prog. Energy Combust. Sci.* **2000**, *26*, 417–458.
- (31) De Soete, G. G. *15th Symposium (International) on Combustion*; The Combustion Institute: Pittsburgh, PA, 1975; pp 1093–1102.
- (32) Perry, S. T.; Fletcher, T. H.; Solum, M. S. *Energy Fuels* **2000**, *14*, 1094–1102.
- (33) Smoot, L. D.; Hill, S. C.; Xu, H. *Prog. Energy Combust. Sci.* **1998**, *24*, 385–408.
- (34) Kandamby, N.; Lazopoulos, G.; Lockwood, F. C.; Perera, A.; Vigevano, L. *Proceedings of the American Society of Mechanical Engineers (ASME) International Joint Power Generation Conference and Exhibition*; Houston, TX, Oct 14–16, 1996.
- (35) Wang, H. J.; Huang, Z. F.; Wang, D. D. *Meas. Sci. Technol.* **2009**, *20*, 1–12.
- (36) Gera, D.; Mathur, M.; Freeman, M. *Energy Fuels* **2003**, *17*, 794–795.